GLOBAL AURORAL IMAGING INSTRUMENTATION FOR THE DYNAMICS EXPLORER MISSION

L. A. FRANK, J. D. CRAVEN, K. L. ACKERSON,
M. R. ENGLISH, R. H. EATHER*, and R. L. CAROVILLANO*
Department of Physics and Astronomy, The University of Iowa, Iowa City, Iowa 52242, U.S.A.

(Received 11 May, 1981)

Abstract. The instrumentation for gaining global images of the auroral oval from the high-altitude spacecraft of the Dynamics Explorer Mission is described. Three spin-scan auroral imaging (SAI) photometers are expected to be able to effectively view the dim emissions from earth in the presence of strong stray light sources near their fields-of-view along the sunlit portion of the spacecraft orbit. A special optical design which includes an off-axis parabolic mirror as the focusing element and super-reflecting mirror surfaces is used to minimize the effects of stray light. The rotation of the spacecraft and an instrument scanning mirror provide the two-dimensional array of pixels comprising an image frame. The full width of the fields-of-view of the photometers corresponding to a single pixel is 0.29°. The angular dimensions of a typical full frame are 30° × 30° and span 1.44 × 10^4 pixels. The images from all three photometers are telemetered simultaneously with a repetition rate that can vary from ~3 to 12 minutes. Two of the imaging photometers provide images of the earth at visible wavelengths, auroral emissions λ391.4 nm, λ557.7 and λ630.0, via interference filters mounted on a wheel and selectable by ground command. In addition filters at other wavelengths are included, such as those at λ317.5 and λ482.5 for measurements of the global distributions of ozone and marine bioluminescence, respectively. Each photometer is capable of observations with any one of a set of twelve filters. The third imaging photometer is equipped with filters and a photocathode for observations at vacuum-ultraviolet wavelengths, in particular emissions of the Lyman-Birge-Hopfield band of N_2 at ~λ140 to λ170. Imaging at these wavelengths will allow coverage of the auroral oval in both the dark and sunlit ionospheres. The filter array for the vacuum-ultraviolet imaging photometer includes also filters for atomic hydrogen Lyα at λ121.6 and the atomic oxygen lines at λ130.4 and λ135.6. The global auroral images at both visible and vacuum-ultraviolet wavelengths are anticipated to greatly increase our knowledge of the interaction of the earth's ionosphere with the magnetospheric plasmas when used in correlative studies with other mission investigations and with supporting ground-based measurements.

1. Introduction

Imaging of auroral emissions from earth satellites is an extremely useful tool in the analyses of observations of the complex plasma phenomena which are encountered at low altitudes over the earth's ionosphere and at the greater distances within the magnetosphere. There are already three sets of such imaging instrumentation that have been successfully operated on earth satellites. ISIS 2 provided auroral images at λ391.4 and λ557.7 (nm) with a photometer and appropriate filters [1]. The two-dimensional array of photometer responses (pixels) comprising an image is obtained via the rotational motion of the spacecraft and the spacecraft orbital motion. The angular resolution of this photometer is 0.4° and the spacecraft altitude is ≈1400 km. A wide-angle (2.5°) scanning photometer for emissions of atomic oxygen at λ630.0 was also included in the complement of ISIS-2 instruments [2]. A second series of auroral images is available

* At Department of Physics, Boston College, Chestnut Hill, Massachusetts 02167, U.S.A.

Space Science Instrumentation **5** (1981) 369–393. 0377–7936/81/0054–0369 $03.75.

from scanning radiometers borne on Defense Meteorological Satellite Program (DMSP) satellites [3]. The two-dimensional pixel array of an image is provided by the orbital motion of the spacecraft and a scanning mirror within the instrument. The effective angular resolution of this imaging device is $\approx 0.25°$. At typical spacecraft altitudes of ≈ 850 km, the spatial resolution at a site of auroral emission directly below the spacecraft is ≈ 3 km. The sensor is a silicon device with broad-band sensitivity extending from about $\lambda 400$ to $\lambda 1130$ [4]. A third type of auroral imaging instrumentation is included in the Japanese satellite KYOKKO [5]. An image-memory tube outfitted with a MgF_2 window and a KBr photocathode is employed to image the auroral oval within the approximate wavelength range $\lambda 120$ to $\lambda 140$ in the vacuum ultraviolet in order to overcome the effects of reflection and Rayleigh scattering of photons which preclude imaging of auroras in the sunlit ionosphere at visible wavelengths. The imaging system views the earth's polar region with an angular resolution of 0.3° in a field-of-view of 60° from altitudes ranging from 650 to 4000 km. Whereas the image repetition rate for the ISIS-2 and DMSP instruments is only one image per orbital period (~ 100 minutes), the KYOKKO imaging device is capable of providing one image every two minutes at vacuum-ultraviolet wavelengths.

We describe here the global auroral imaging instrumentation for the Dynamics Explorer Mission to be flown on the high-altitude spacecraft. Two imaging photometers are employed for measurements at visible wavelengths, one such photometer for vacuum-ultraviolet wavelengths. These instruments use scanning mirrors and the spacecraft rotational motion to provide the two-dimensional array of pixels which comprise an image. The sensors are photomultipliers with appropriate windows and photocathodes for image capability at both vacuum-ultraviolet and visible wavelengths. These wavelengths include hydrogen Lyα at $\lambda 121.6$, O I lines $\lambda 130.4$ and $\lambda 135.6$, the LBH band of N_2 at $\approx \lambda 140$ to $\lambda 170$, the N_2^+ (0–0) band at $\lambda 391.4$, and O I lines $\lambda 557.7$ and $\lambda 630.0$. The angular size of a full image frame is $120° \times 30°$ with a pixel dimension of about 0.25°. The frame repetition rate is dependent upon the instrument operating mode, and whether full or partial frames are telemetered, but is generally in the range ≈ 3 to 12 min per frame for each imaging photometer. Images from the three photometers are obtained simultaneously. These images will be gained at spacecraft altitudes of $\approx 1\ R_E$ to $4\ R_E$. It is to be noted here that global auroral imaging at visible wavelengths is required along the sunlit portions of the spacecraft orbit. Hence special optical systems are used in order to provide the capability of viewing the relatively weak auroral emissions with intensities $\approx$ kilorayleighs and less with the intense light from the sunlit ionosphere, $\approx 5 \times 10^5$ kR nm^{-1}, near or within the fields-of-view of the instruments' collimators. The scattered light from this intense source, the sunlit ionosphere, is minimized via the use of off-axis parabolic mirrors and super-reflecting optical surfaces.

The greatly enhanced imaging capabilities of this instrumentation relative to those of previously flown instruments, combined with the extended viewing periods with the high-altitude orbit and the comprehensive *in situ* measurements of plasma and ionospheric phenomena provided by other instruments on both high-and low-altitude spacecraft, offer an exciting opportunity to substantially increase our knowledge of magnetospheric

and auroral dynamics. Several of these broad scientific objectives are (1) to establish and clarify the association of diverse auroral emission features with the auroral and magnetospheric plasmas, (2) to determine the relationship between vacuum-ultraviolet and visible auroral emissions, (3) to determine the evolution of the auroral oval during magnetic substorms by taking advantage of the temporal resolutions of the imaging photometers and the extended viewing times wih the high-altitude orbit, and (4) to develop global models for field-aligned currents, ionospheric convection and charged-particle precipitation during all conditions of magnetic activity. Indeed such imaging will provide a natural coordinate system, and a monitor of magnetospheric and ionospheric activity, to reference *in situ* point measurements with both spacecraft and thus allow truly global analyses of our near-earth plasma environment.

2. Instrument Description

The optical and electrical designs of the imaging photometers are sufficiently numerous and complex that we are limited here to providing only a discussion of the overall design, although in sufficient detail for the reader to interpret principal features of the variety of images which may be acquired with this instrumentation.

2.1. Acquisition of the Pixel Array

The viewing geometry for one of the three imaging photometers is shown diagrammatically in Figure 1. The field-of-view of the photometer is conical with full angle of 0.32° (5.6 millirads). The direction of this field-of-view is controlled via a scanning mirror within the instrument. This field-of-view is rotated in 0.25° increments in a plane containing the spacecraft spin axis and a vector directed perpendicular to the spin axis, i.e., in a spacecraft meridional plane. The full angle for the scan of the field-of-view is 30° and its axis is centered perpendicular to the spin axis. The incremental rotation of the mirror and the spacecraft rotation are thence utilized to acquire the two-dimensional pixel array that comprises an image. In the left-hand side of Figure 1 are shown the ground tracks of the field-of-view for two successive rotations of the spacecraft. The incremental rotation of the instrument scanning mirror must be synchronized with the spacecraft rotation. This synchronization is implemented via nadir pulses derived from spacecraft infrared horizon sensors. At spacecraft altitudes exceeding 2.8 R_E (R_E, Earth Radius), the instrument field-of-view is sufficient to acquire an image of the entire earth (the auroral zone subtends a considerably smaller angle). In order to acquire and telemeter such a full frame with 30° angular width, 120 spacecraft rotations at 6 s per rotation, or 720 s, are required. The frame repetition rate is directly proportional to the angular width of the image frame. Note also in Figure 1 that the terminator is in view from the spacecraft, which necessitates the special optical design as discussed in a following section in order to view the relatively very weak auroral emissions at visible wavelengths in the presence of a large source of stray light from the sunlit ionosphere. The three imaging photometers are positioned such that their fields-of-view are oriented at $\approx 120°$ relative to each other in a plane perpendicular to the spacecraft spin axis. This

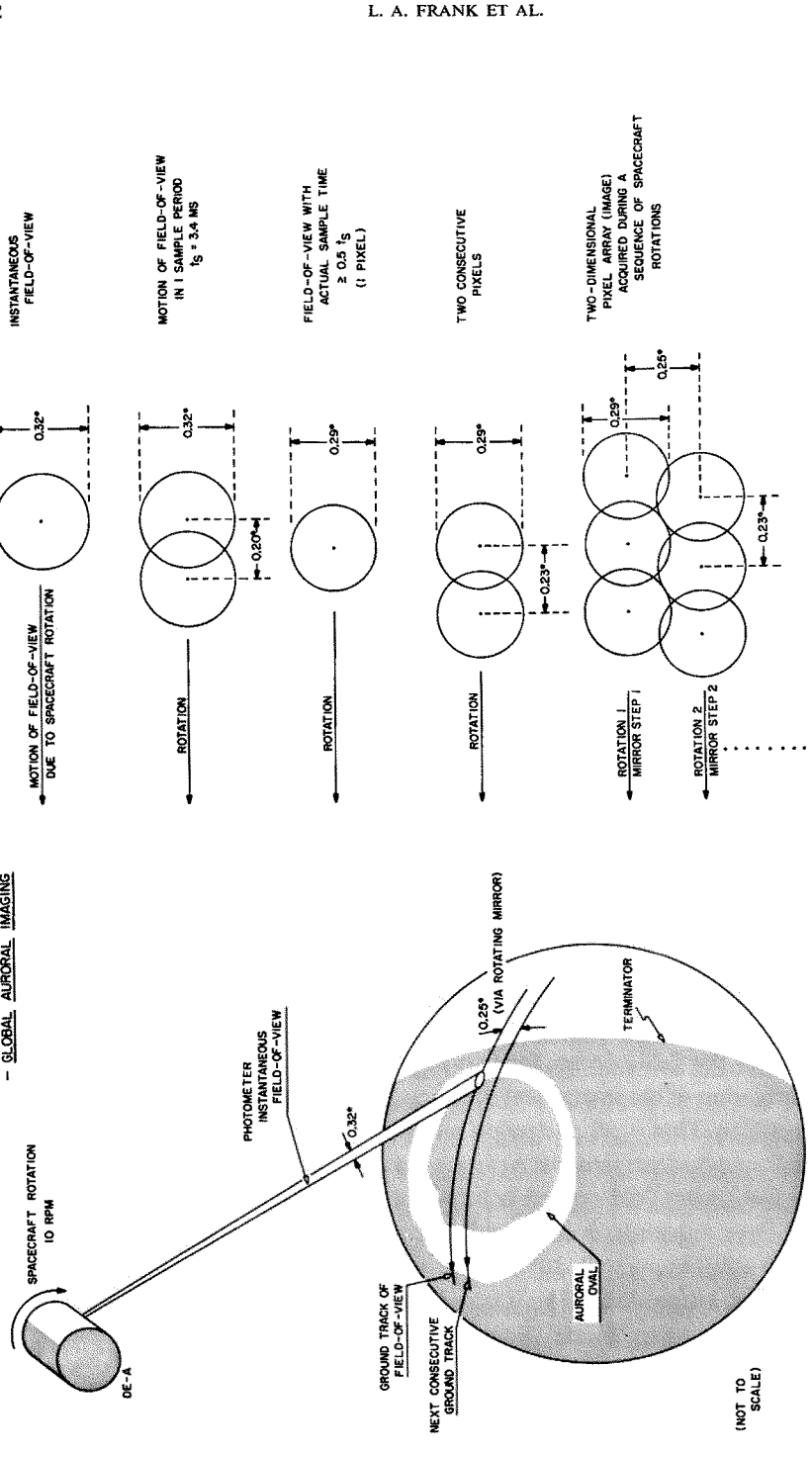

Fig. 1. Diagram showing the viewing geometry of one of the three auroral imaging photometers relative to the auroral oval. The corresponding angular dimensions of a single pixel and of successive pixels which comprise an image frame are given in the right-hand side of this figure.

arrangement allows three auroral images, one each for the three photometers, to be telemetered simultaneously with a minimum bit-rate requirement.

The details of the relationship between the imaging photometer field-of-view and the pixel array forming an image are summarized in the right-hand side of Figure 1. The angular width of the photometer field-of-view is 0.32°. Responses of the photometer are accumulated for a 3.4-ms period corresponding to a spacecraft rotation of 0.20°. This sampling period for one pixel corresponds to an approximately conical field-of-view with

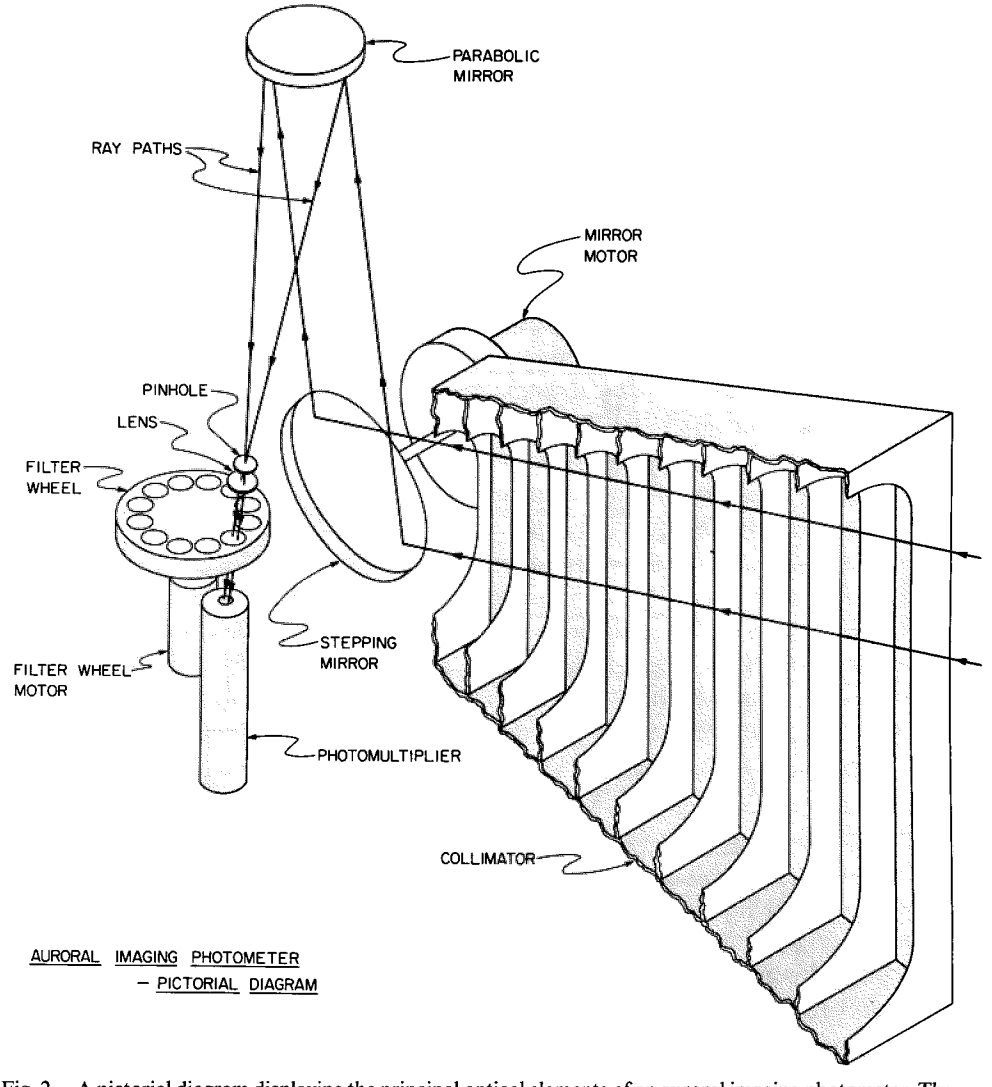

Fig. 2. A pictorial diagram displaying the principal optical elements of an auroral imaging photometer. The surfaces of the stepping mirror and parabolic focusing mirror are super-reflecting, i.e., highly polished surfaces of electroless nickel.

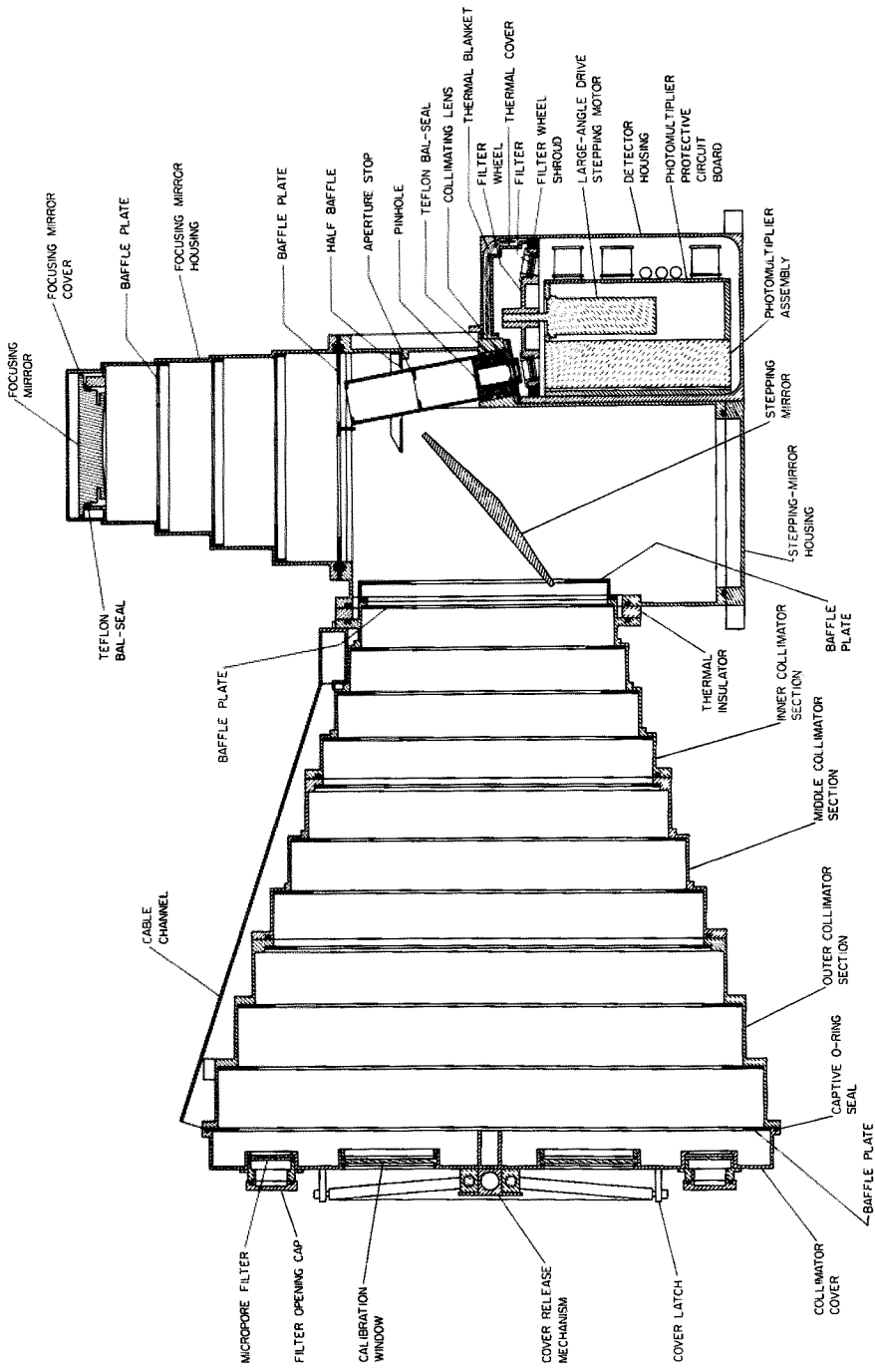

Fig. 3. Detailed mechanical drawing of the cross-section of an imaging photometer in the plane containing the optical chief ray.

full angle 0.29° for which the sample time within this field-of-view is equal to or exceeds 1.7 ms. The angular separation of two consecutive pixels in the direction of spacecraft rotation, including electronic dead-times, is 0.23°. Each such row of pixels is separated by 0.25°. However, the relative phase of the pixels from rotation to rotation is time-dependent and is determined from aspect sensors mounted on the spacecraft.

2.2. Principal Optical Elements

The principal optical elements of an auroral imaging photometer are displayed in the pictorial diagram of Figure 2. The primary collimator is equipped with knife-edged baffle plates which are surface-coated with Martin Optical Black Coating by Martin-Marietta Corporation. The aperture stop which prevents the photomultiplier tube from viewing these knife edges is shown in Figure 3. The stepping (scanning) and parabolic (focusing) mirrors are constructed from beryllium stock and surfaced with highly polished, electroless-nickel plating. Aluminium is vacuum-deposited over the nickel surface to increase reflectivity. Protective overcoats are SiO_2 for the visible imaging photometers and MgF_2 for the vacuum-ultraviolet photometer. These mirrors are provided by Speedring, Inc. The stepping mirrors are rotated in 0.125° increments with a permanent-magnet stepper motor with a harmonic drive speed reducer which is supplied by Schaeffer Magnetics, Inc. The effective collecting area for the optics is 20.3 cm^2. This collecting area, and hence the sensitivity of the imaging photometer, is generally limited by the dimensions of the collimator and the focal length that can be accommodated by a given spacecraft; optical systems with such dimensions are fitted into the Dynamics Explorer spacecraft.

There are three primary optical elements that are required in order to minimize the stray light scattering in the instrument when the mirrors are illuminated by intense light from the sunlit ionosphere. These elements are (1) a long, effective collimator for minimization of the solid angle of the sunlit ionosphere as seen at the stepping mirror, (2) a primary optical system for which only optical surfaces lie in the light paths and (3) super-reflecting optical surfaces. The requirement of no obstructions in the primary light path precludes the use of a telescope with a Cassegrain or a Coudé focus, for example. Thus we chose an off-axis section of a parabolic mirror for the focusing element of the imaging photometer. The focal length of the mother parabolic reflector is 19.9 cm. Computer software for ray tracing is used to verify that the angular resolution of this optical system is sufficient for the desired angular resolution of 0.32°. In terms of blur profile dimensions in the focal plane, the diameter of the blur circle containing 90% of the energy from a parallel beam is <40 μm from aberrations and <4 μm from Fraunhofer diffraction. Since the diameter of the pinhole in the focal plane is 1130 μm, the focusing properties of this optical system are more than sufficient for the angular resolution of the instrument. These mirrors are finished with a super-reflecting surface that provides excellent reduction of wide-angle (several degrees) scattering of light relative to standard high-grade optical surfaces. For example, the scattering of light at 5° from the direction of a specularly reflected beam is measured to be at least a factor of 1000 less for such mirrors relative to the scattering from commercial laboratory aluminum mirrors.

The pinhole, a collimating lens, filter wheel and its drive motor, and a photomultiplier

tube comprise the focal-plane optical assembly. The angular resolution of the photometer is defined by the pinhole diameter. This pinhole is in the focal plane of a small collimating lens which provides a light beam of small angular divergence at the filter wheel. The collimating lens is necessary to reduce the loss of sensitivity due to beam divergence, particularly in the case of the narrow-passband filters at visible wavelengths. These $f/1.7$ lenses are constructed from Suprasil-1 and MgF_2 for the visible and vacuum-ultraviolet photometers, respectively, by Muffoletto Optical Company, Inc. The filter wheel provides accommodations for twelve filters and is driven with a permanent-magnet stepping motor which is coupled to the filter wheel via a combination spur and planetary gear train. This filter wheel motor assembly is supplied by MPC Products Corporation. Twelve filters are mounted in the filter wheel of each imaging photometer. Interference filters for the two visible imaging photometers are deposited on Dynasil-1000 substrates and include out-of-passband rejection filters. These filters are constructed by Barr Associates, Inc. The vacuum-ultraviolet filters comprise both narrow-band interference filters and BaF_2, CaF_2 and MgF_2 windows which are supplied by Acton Research Corporation. An aluminum flashing is applied to the windows in order to suppress the long-wavelength transmission, an important feature for vacuum-ultraviolet measurements when the instrument is viewing the sunlit ionosphere. EMR Photoelectric Division miniature photomultiplier tubes are selected as sensors. Models 510E-01-13 and 501G-09-13 are used for the visible and vacuum-ultraviolet imaging photometers, respectively. At visible wavelengths a fused-silica window with a semi-transparent tri-alkali photocathode is employed, at vacuum-ultraviolet wavelengths the window is MgF_2 of vacuum-ultraviolet quality and the photocathode is CsI. These photomultipliers are each accompanied by a high-voltage power supply, high-gain wide-band amplifier and a fixed-threshold pulse shaper (EMR Model 717U-00).

2.3. Details of the Mechanical Assembly

The cross-sectional view of an imaging photometer as taken in the plane containing the chief ray is shown in Figure 3. The approximate overall dimensions are 54 cm (length) and 38 cm (height) in the plane of the figure and a depth of 24 cm. The volume which houses the primary optics and extends from the collimator cover to the collimating lens is hermetically sealed with captive O-rings and teflon Bal-seals in order to protect the surfaces of the super-reflecting mirrors from particulate and vaporous depositions. This part of the instrument is assembled in a special Class 100 clean room at the University of Iowa. The collimator cover is to be released approximately two weeks after orbital insertion of the spacecraft. This cover is secured to the collimator by four latches which are held closed via spring-loaded pistons forced apart by a biphenyl slug. Sublimation of the biphenyl is controlled by the dimensions of an outgassing hole in the housing for the slug. The cover release time as a function of temperature and of outgassing hole size was determined during extensive laboratory work in a vacuum chamber. A fail-safe is included in the release mechanism in the form of a heater which is activated by ground command and is capable of sublimating the biphenyl within several tens of minutes. Micropore filters are also included in the collimator cover to equilibrate the instrument

interior and environmental pressures during thermal vacuum testing and launch operations. Normally the filters are covered with hermetically sealed caps. Microswitches that indicate proper release of the cover, and collimated photodiodes that sense the presence of the sun within the primary field-of-view of the instrument, are mounted on the outer face of the collimator but are not shown in the diagram of Figure 3. During spacecraft thermal-vacuum testing, nonflight mirrors are used for the visible imaging photometers due to the presence of heavy organic molecules from the diffusion pumps of the test facility. The super-reflecting mirrors are installed just prior to launch. Due to the significantly lesser intensities of stray light sources at ultraviolet wavelengths such surface degradation is not expected to be as serious for the vacuum-ultraviolet imaging photometer; however these mirrors are carefully inspected after environmental testing.

The large collimator is thermally insulated from the optics and electronics housing in order to implement both spacecraft and instrument temperature design goals. Due to the necessarily high thermionic electron emission from the tri-alkali photocathodes, the

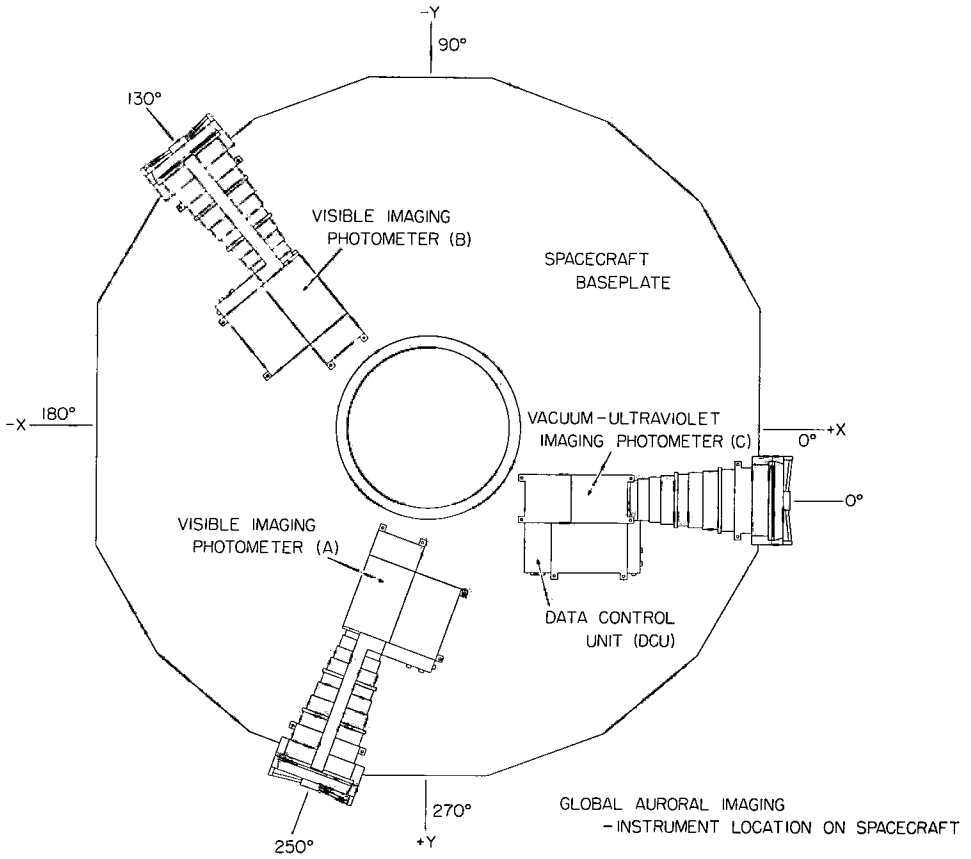

Fig. 4. Definition of the directions of the fields-of-view of the three imaging photometers relative to the spacecraft-fixed coordinate system. The spacecraft spin axis is directed perpendicular to the plane of the figure. Photometers A and B provide images at visible wavelengths, photometer C at vacuum-ultraviolet wavelengths.

desired highest temperature for operating the corresponding photomultipliers is $\sim 15\ ^\circ C$. In addition the temperature of the filter wheels for the visible imaging photometers must be controlled due to the presence of several filters with passbands of only 0.3 nm and a temperature sensitivity of 0.02 nm $^\circ C^{-1}$. This temperature control is provided by a thermal blanket and a thermostatically controlled heater.

2.4. Instrument Mounting on Spacecraft

The directions of the fields-of-view of the three imaging photometers and the instruments' locations relative to the spacecraft baseplate and coordinate system (X, Y) are summarized in Figure 4. An attempt at orienting these fields-of-view at angular separations of precisely 120° is prevented by obstruction from the spacecraft structure and support systems. However, the actual angular separations of 130, 120, and 110° are sufficiently equal as to have no effect on the auroral image coverage of the three instruments as their outputs are sequentially commutated as a function of spacecraft rotation phase into shared telemetry lines. Mirrors permanently mounted to each of the imaging photometer housings are used to determine the instruments' fields-of-view relative to the spacecraft coordinate system, and hence relative to those of the attitude sensors, with an accuracy of $\pm 0.05^\circ$.

2.5. Imaging Photometer Electronics

A block diagram which displays the major electronic elements of each of the three imaging photometers is shown in Figure 5. In Figure 5(a) are shown the protective circuits that are employed in order to protect the photomultiplier tube from damage as it views strong light sources. The outputs of two redundant phototransistors mounted in the outer face of the collimator are used to trigger a protective circuit when the sun is within the field-of-view of the imaging photometer. This protective circuit supplies a blocking voltage to the photocathode of the thirteen-stage photomultiplier tube, and the second dynode is grounded simultaneously, such that electrons emitted by the photocathode are unable to reach the dynode and hence initiate the multiplication process in the dynode string. Thus damage to the final dynodes due to excessive current densities is prevented. The phototransistor sensitivities can be varied by ground command in the situation that there is gain degradation due to radiation damage or other effects. The thresholds are set such that the sun, but not the sunlit earth, will activate the protective circuit. A second protective measure is taken by continuously sampling the pulse rate of the photomultiplier with a shifting accumulator at intervals of 1.1 ms. When the contents of this counter exceed a prelaunch determined value, the protective circuit is activated. This rate is 480 kHz. A third protective feature available for the photomultiplier is ground-command control of the angular range for the stepping mirror as discussed below (Figure 5(b)). The gain of the photomultiplier tube may be changed to one other value by ground command in the circumstance that its response-versus-voltage characteristic changes after launch. Also shown in Figure 5(a) is the manner in which the photometer responses are encoded into the spacecraft telemetry stream. The photometer responses are fed into two 7-bit semi-logarithmic compressors with a dynamic

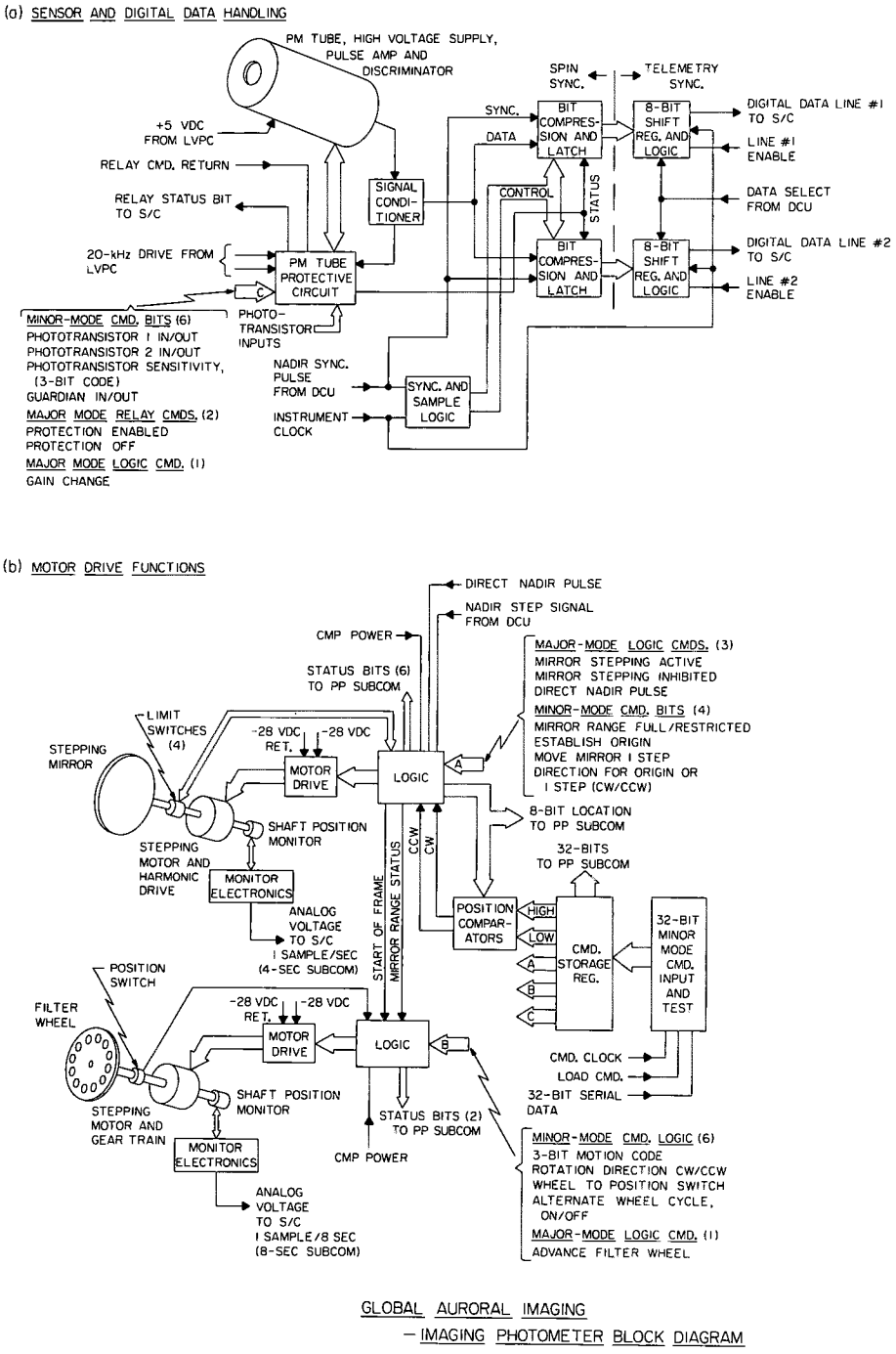

Fig. 5. Partial electronics block diagram for an imaging photometer. The electronics for all three photometers are identical with the exception of the omission of a filter heater for thermal control in photometer C.

range of a factor of 1600. The eighth bit of each word is used to indicate whether or not the protective circuit was activated during each 3.4-ms sample of photometer responses. The outputs of each of the compressors and the status of the protective circuit are transferred to an 8-bit shift register and are subsequently fed into the spacecraft telemetry stream on demand from an enable signal. Thus two successive photometer samples are each transferred to separate spacecraft digital data lines. This scheme allows passage of 50% of the image (alternate pixels) in the event of failure of a bit compressor, 8-bit register or digital data line. All three photometers share these two spacecraft digital data lines. Determination of the dedication of these two data lines to a given imaging photometer as a function of spacecraft rotation phase is provided by the data control unit (DCU).

An overview of the electronics associated with the two motors, i.e., stepping mirror and filter wheel motors, is given in Figure 5(b). By ground command the stepping mirror motor electronics can provide continuous, cyclic stepping of the mirror over its full viewing range or any restricted (partial) angular range. For a restricted stepping sequence the angle of origin and the magnitude of the angular scan can be specified. The mirror is rotated sequentially clockwise and counterclockwise between the two angular limits. The angular position of the mirror is normally incremented once per spacecraft rotation via the nadir pulse. However it is possible to rotate the mirror one increment, clockwise or counterclockwise, per minor-mode ground command for diagnostic purposes. The mirror position is monitored with an 8-bit location counter in the digital control electronics. Knowledge of a reference position for the motor shaft is given to the digital logic via two sets of two magnetically activated reed switches which are positioned such that their closures coincide with the shaft positions corresponding to the angular limits of the field-of-view of the imaging photometer. These are indicated as limit switches in Figure 5(b). An independent verification of the mirror position is provided by a shaft potentiometer. This analog voltage is supplied to the analog performance parameter subcommutator. The functions for the electronics associated with the filter-wheel motor are similar to those for the stepping mirror motor. Since the filter wheel is usefully rotated 360°, the limit switches which are employed by the stepping motor shaft are replaced by a single pair of reed switches for the filter wheel shaft. The above capabilities of the stepping mirror and filter wheel rotational modes allow flexible and adaptable formats for imaging, i.e., individual frame sizes for each imaging photometer, sequential sets of wavelengths for the images, and directions of fields-of-view in response to spacecraft orbital position.

2.6. Electronics for the data control unit (DCU)

The principal functions of the data control unit are to supply nadir pulses to the imaging photometers and to commutate the responses of the three imaging photometers, as each views the earth, onto the spacecraft digital data lines. These functions are summarized in the electonics block diagram of Figure 6. Two sets of nadir pulses are received from the spacecraft. One nadir pulse group allows each of the three imaging photometers access to the digital data lines for 120° of spacecraft rotation and with the corresponding

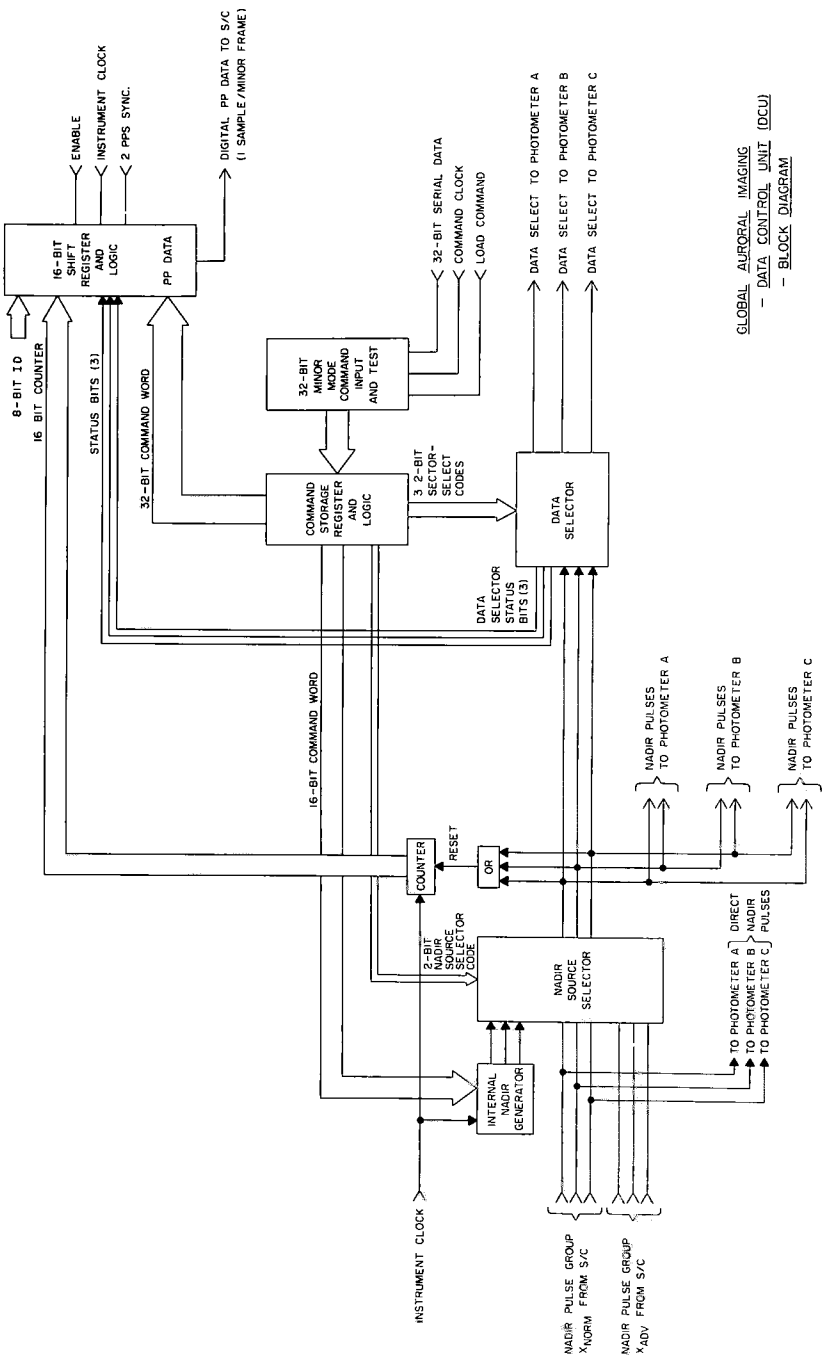

Fig. 6. Electronics block diagram for the data control unit which provides nadir pulses for incremental rotation of the photometer mirrors and data select pulses to allow sharing of two spacecraft digital data lines by all three imaging photometers. Since this is the only instrument electronics subsystem that is shared by the three photometers a failure circumvention mode is provided, which completely bypasses the data control unit and still allows normal acquisition of images from a single photometer.

view of earth approximately centered within this 120° frame. The second nadir group is identical except delayed in phase by 60°. In the event of failure of the spacecraft electronics to provide either of these two nadir groups it is possible to use a nadir pulse group that is generated by an internal nadir generator. The frequency of these nadir pulses is approximately tuned to the spacecraft rotation rate by adjustments to the frequency of an internal oscillator via a 32-bit minor mode command. Ground commands to the nadir source selector are used to select among the above three nadir pulse groups. In addition the assignment of a given photometer to any one of the 120° angular segments of rotation can be implemented by ground commands to the data selector for further viewing flexibility. In order to insure that there is no failure mode of the data control unit that would totally prevent the acquisition of images from the three photometers, the normal group of spacecraft nadir pulses is also directly routed to the imaging photometers. In the event of complete failure of the data control unit, imaging from any one of the three photometers is continued by denying power to the other two photometers. In this mode the responses of the selected photometer are sampled for the entire 360° of spacecraft rotation.

2.7. Mass and power

The mass of each of the three imaging photometers is 7.2 kg, and the mass of the data control unit which is attached to the vacuum ultraviolet photometer is 0.6 kg. Thus total instrument mass is 22.2 kg. Each imaging photometer consumes 0.84 watt during normal operation without heater usage for a total of 2.55 W. An additional 1.75 W are required for each of the two visible imaging photometers if heating of the narrow-band interference filters is necessary.

3. Calibrations

3.1. Visible imaging photometers

The passbands of the interference filters for the visible imaging photometers are measured with a 1-meter SPEX Model 1704 monochromator for filters with passband widths $\leqslant 2$ nm and a CARY 14 dualbeam double monochromator for the filters with passbands > 2 nm. Filter transmissions are determined by comparing these responses with those obtained via monochromator reruns without filters. The absolute sensitivity of the imaging photometers for each filter is then calculated with known mirror reflectivities, collimating lens transmissions and photomultiplier quantum efficiencies at the respective wavelengths for a pinhole diameter of 1130 μ. These calculated values for the absolute sensitivities of the imaging photometers are then verified with instrument responses to a broad-band diffuse light source which is calibrated against a secondary NBS standard over the wavelength range extending from λ300 to λ800. The calculated and measured values for absolute sensitivities are in agreement within 10%. Absolute sensitivities of imaging photometer B as functions of wavelength in units of nanometers for six of its filters are shown in Figure 7. The units of these sensitivities are counts/kilorayleigh-pixel.

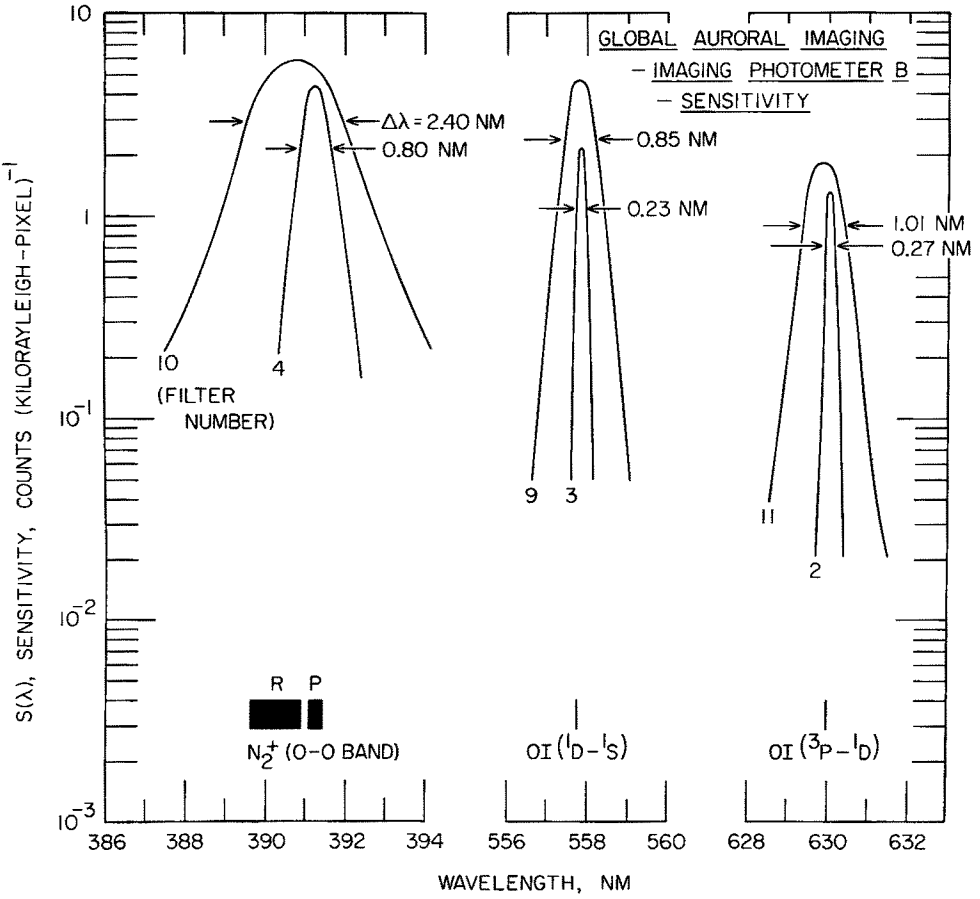

Fig. 7. The absolute sensitivities of visible imaging photometer B as functions of wavelength for six of the twelve filters in its filter wheel.

For example if filter 9 is used to view an aurora with brightness 1 kilorayleigh of atomic oxygen $[OI]_{32}$ emission then the photometer response will be 4.8 counts per pixel. The absolute sensitivities of all three imaging photometers after launch will be monitored periodically by utilizing the responses of the photometers to several bright stars within their fields-of-view.

3.2. Vacuum-ultraviolet imaging photometer

The absolute responses of the vacuum-ultraviolet imaging photometer as functions of wavelength for each of the twelve filters on the filter wheel are measured with the instrument mounted on an optical bench in a vacuum chamber. The light source is a McPherson Model 630 vacuum-ultraviolet source fed with a hydrogen gas bleed and is followed by a 0.3-meter McPherson Model 218 monochromator. An EMR Photoelectric Model 542G-08-18 photomultiplier tube is employed as a beam monitor. This beam

monitor is subsequently calibrated in the wavelength range λ113 to λ350 with a NBS secondary standard, an EMR photodiode with a rubidium-telluride photocathode, Model 543P-09-00. The absolute sensitivities of the vacuum-ultraviolet imaging photometer for six of its filters as functions of wavelength are given in Figure 8. For example, filter 8 is a narrow-band filter intended for imaging hydrogen Lyα at λ121.6, and filters 4 and 5 are sufficiently insensitive to these shorter wavelengths to effectively image auroral emissions in the molecular nitrogen LBH band from both the dark and sunlit ionospheres. The background responses of the imaging photometer, which are attributable to longer wavelength light > λ250, can be estimated from the terrestrial backscatter spectrum and the measured photometer responses at these wavelengths. For a worst-case estimate the photometer responses for filter 5 (see Figure 8) to the sunlit ionosphere

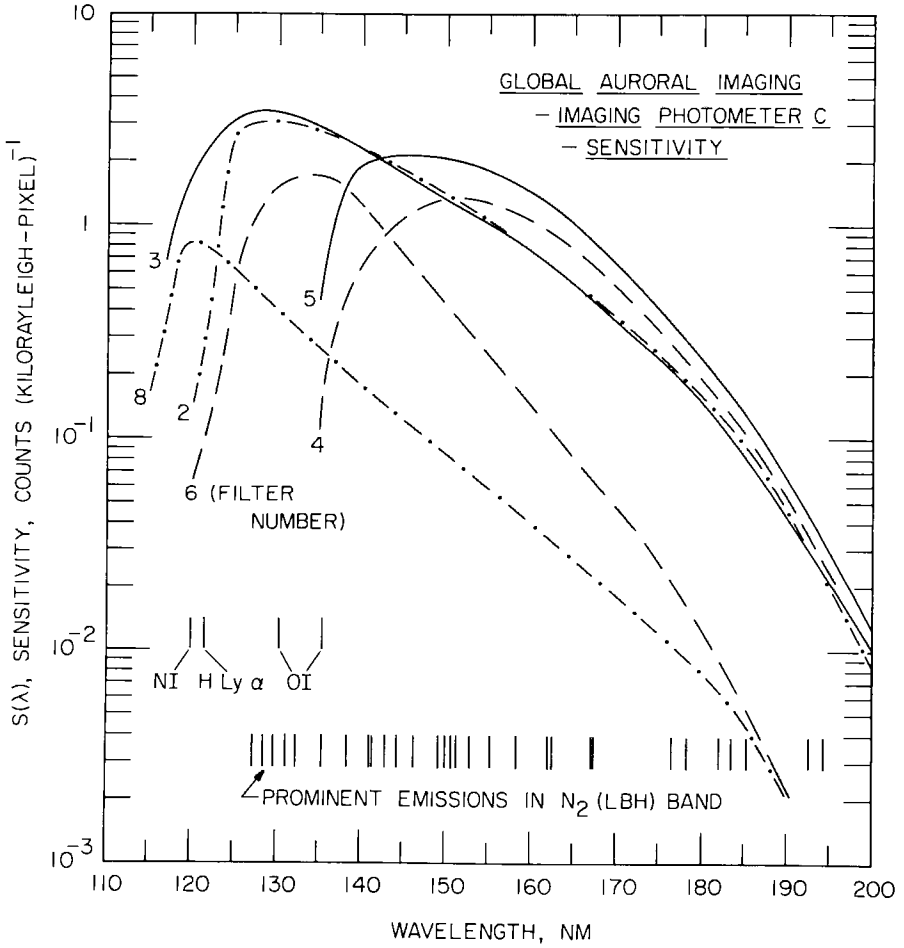

Fig. 8. The absolute sensitivities of vacuum-ultraviolet imaging photometer C as functions of wavelength for six of the twelve filters in its filter wheel. Filters 4 and 5 are employed for images of auroral emissions from both dark and sunlit ionospheres, filter 8 for hydrogen Lyα emissions and scattered solar intensities in the exosphere.

at the equator and a solar zenith angle of 0° are found to have two maxima at λ200 to λ210 and λ310 to 330 nm, respectively. The corresponding estimated responses are ~15 and 3 counts/pixel, respectively. The absence of a significant contribution over wavelengths λ220 to λ300 is due to absorption in the Hartley continuum of O_3. The background rates for narrowband filter 8 are expected to be lesser by factors ~20. These background rates will decrease for increasing latitudes and increasing solar zenith angles such that responses due to auroral emissions in the sunlit ionosphere for filters 4 and 5 should exceed contributions due to longer-wavelength backscattered radiation by ~2 to 10 counts/pixel.

3.3. Stray Light Effects

The imaging photometers are designed to provide usable images of the auroral oval in the presence of relatively intense sources of scattered light from the sun, sunlit ionosphere and the moon. This stray light contamination is a primary consideration for the visible imaging photometers since solar intensities at vacuum-ultraviolet wavelengths are lesser by orders of magnitude. The effectiveness of the photometers in achieving this substantial requirement relies principally upon the design of the collimator baffles and primary optics and on the low scattering coefficients of the super-reflecting optical surfaces. Consider an auroral intensity of 1 kilorayleigh with the sun directly illuminating the first mirror at an angle of 5° to the direction of the auroral emission. The corresponding signal-to-noise (S/N) ratio is in the range 4×10^{-4} to 4×10^{-2}. The lower value corresponds to an upper limit which is determined by our laboratory measurements for the scattering from a sample mirror; the upper limit corresponds to the manufacturer's best specification. Hence auroral imaging is not possible if the sun is directly illuminating the primary optics. However, this situation arises only during a relatively small fraction of the DE mission. If the sun is illuminating only the outer baffle edges, the corresponding S/N is 5×10^2 to 5×10^4 and auroral imaging is within the capabilities of the instrument. If the full moon is illuminating the primary optics the corresponding range of S/N for a 1-kilorayleigh aurora at a moon-spacecraft-aurora angle of 5° is 4×10^2 to 4×10^4. Again auroral imaging is easily possible for this situation. Finally we consider the S/N ratios for a terminator-spacecraft-aurora angle of 2° and an auroral intensity of 1 kilorayleigh. The corresponding range of S/N values is 0.2 to 20. Even with the most pessimistic value of 0.2, the instrument will allow usable global imaging of the auroral oval during the sunlit portions of the spacecraft orbit. Recent measurements of test samples of optical finishes representative of those for the flight mirrors indicate that the S/N values will be considerably better than these pessimistic lower limits.

4. Operating Modes

There is a considerable amount of versatility available in the inflight operation of the three imaging photometers. In general each spacecraft orbit or a series of orbits is to be assigned a primary imaging objective, and a particular set of ground commands which is tailored to achieve this objective is sent to the spacecraft command sequencer. The

scope of these scientific objectives is broad and ranges from viewing the global evolution of an auroral substorm at three wavelengths simultaneously to surveys of marine bioluminescence.

In the design of a particular imaging mission with the Dynamics Explorer instrumentation there are several ground rules to be considered. Images are telemetered from three imaging photometers simultaneously. The angular width of an imaging frame, i.e., the angular scan of the stepping mirror, is 30°. When three photometers are operated simultaneously, responses of each photometer for 120° of spacecraft rotation are telemetered. Hence the overall angular dimensions of a frame are 30 × 120°. If the responses of only one imaging photometer are telemetered, then angular coverage of 360° of spacecraft rotation yields frame dimensions of 30 × 360°. Within the 30° scanning capability of an imaging photometer the field-of-view is rotated in 0.25° increments each spacecraft rotation period, or a total of 120 angular increments. This scanning motion of the mirror can be limited via ground command to any angular segment within the 30° field-of-view. For example, an image with width 15° can be centered within the field-of-view and requires only 60 angular increments of the stepping mirror. The frame repetition rate is dependent upon the width of the frame and the spacecraft rotational period. The nominal spacecraft rotation period is 6 s (10 rpm). Hence a full image frame of 30° requires an observing period of 120 scans × 6 s, or 720 s. The two visible imaging photometers can be used to reduce this frame repetition period to 360 s by using filters with common passbands on their respective filter wheels. If image frames of 15° in width are selected then the frame repetition period further reduces to 180 s. The minimum spacecraft altitude for routine imaging is approximately 1 R_E. Images taken at lesser altitudes will be significantly distorted by the rapidly changing altitudes, and aspect of the earth as seen from the spacecraft, that occur near perigee. The spatial resolution of a pixel at auroral altitudes in the nadir direction is 28 km at a spacecraft altitude of 1 R_E; near apogee at altitude 3.9 R_E this resolution is 109 km. With special processing and considerable effort, images from somewhat lesser altitudes may be constructed if there is sufficient scientific promise. Each imaging photometer is capable of providing successive frames at different wavelengths via the filter wheel. For example, a single imaging photometer can be used to obtain successive frames of the auroral oval at λ391.4, λ557.7 and λ630.0, respectively.

Twelve optical filters are mounted on the filter wheel of each imaging photometer. The passbands of these filters and the absolute sensitivities of the imaging photometers A, B, and C at these corresponding wavelengths are summarized in Tables I, II and III, respectively. There is a complete set of filters for the atomic oxygen lines λ557.7 and λ630.0 and the singly-ionized molecular nitrogen band centered at λ391.4 in each of the filter wheels for visible imaging photometers A and B. These filters include filters with moderate and narrow passbands at each of the above wavelengths. For example, the transmittance of moderate-resolution passband filter 4 (photometer A, Table I) for the $[OI]_{32}$ emission is a factor of 1.85 greater than that for the corresponding narrow passband filter 9. Since the ratio of passband widths of these two filters is 0.32, the signal-to-noise ratio in the presence of stray light and earth-reflected moonlight, etc.,

TABLE I

Photometric sensitivities and filter properties (visible imaging photometer A)

Filter (No.)	λ_p (nm)	$\Delta\lambda$ (nm)	T_p	S_p	Function
1	360.0	3.00	1.9×10^{-5}	2.3×10^{-4}	Surface albedo for ozone measurements
2	317.5	3.00	3.9×10^{-5}	5.7×10^{-4}	Total ozone
3	630.03	1.06	0.45	0.88	$[OI]_{21}$ line
4	557.80	0.90	0.48	2.40	$[OI]_{32}$ line
5	390.85	2.36	0.27	3.31	N_2^+(0-0) band
6	394.96	1.20	0.16	1.96	Background for λ391.4
7	626.57	1.10	0.55	1.08	Background for λ630.0
8	630.07	1.08	0.40	0.78	$[OI]_{21}$ line
9	557.87	0.29	0.26	1.30	$[OI]_{32}$ line (narrow Δλ)
10	391.30	0.85	0.19	2.33	N_2^+(0-0) (narrow Δλ) centered on band head
11	630.06	0.26	0.34	0.66	$[OI]_{21}$ line (narrow Δλ)
12	557.77	0.26	0.32	1.60	$[OI]_{32}$ line (narrow Δλ)

λ_p is wavelength at peak transmission for filter.
$\Delta\lambda$ is passband FWHM.
T_p is transmission at λ_p and + 15 °C.
S_p is sensitivity at λ_p in units of counts/(kilorayleigh-pixel).

TABLE II

Photometric sensitivities and filter properties (visible imaging photometer B)

Filter (No.)	λ_p (nm)	$\Delta\lambda$ (nm)	T_p	S_p	Function
1	629.76	1.17	8.0×10^{-5}	3.2×10^{-4}	Daylight cloud filter
2	630.05	0.27	0.31	1.31	$[OI]_{21}$ line (narrow Δλ)
3	557.82	0.23	0.23	2.40	$[OI]_{32}$ line (narrow Δλ)
4	391.24	0.80	0.20	4.49	N_2^+(0-0) (narrow Δλ), centered on band head
5	630.04	0.26	0.28	1.19	$[OI]_{21}$ line (narrow Δλ)
6	317.50	3.00	3.9×10^{-5}	1.0×10^{-3}	Total ozone
7	482.50	44.0	0.45	7.40	Marine bioluminescence
8	554.63	0.85	0.39	3.85	Background for λ557.7
9	557.82	0.85	0.47	4.85	$[OI]_{32}$ line
10	390.80	2.40	0.26	5.84	N_2^+(0-0) band
11	629.97	1.01	0.44	2.00	$[OI]_{21}$ line
12	557.78	0.90	0.47	4.64	$[OI]_{32}$ line

λ_p is wavelength at peak transmission for filter.
$\Delta\lambda$ is passband FWHM.
T_p is transmission at λ_p and + 15 °C.
S_p is sensitivity at λ_p in units of counts/(kilorayleigh-pixel).

TABLE III

Photometric sensitivities and filter properties (vacuum-ultraviolet imaging photometer C)

Filter (No.)	λ_p (nm)	$\Delta\lambda$ (nn)	T_p	S_p	S(Lyα)	Principal function
1	150	43	0.21	1.65		N_2(LBH) band
2	131	32	0.30	3.08		OI lines
3	125	30	0.36	3.10	2.18	H Lyα line
4	156	34	0.18	1.27		N_2(LBH) band (narrow $\Delta\lambda$)
5	150	41	0.25	2.05		N_2(LBH) band
6	135	18	0.17	1.71		OI lines (narrow $\Delta\lambda$)
7	128	30	0.30	3.08		OI lines
8	120	11	0.13	0.84	0.79	H Lyα line (narrow $\Delta\lambda$)
9	154	43	0.17	1.26		N_2(LBH) band (narrow $\Delta\lambda$)
10	129	14	0.18	1.80		OI lines (narrow $\Delta\lambda$)
11	120	11	0.14	0.91	0.79	H Lyα line (narrow $\Delta\lambda$)
12	130	47	1.00	10.5	7.0	H Lyα line

λ_p is wavelength of peak transmission for filter.
$\Delta\lambda$ is passband FWHM.
T_p is transmission at λ_p.
S_p and S(Lyα) are the sensitivities at λ_p and λ121.6, respectively, and are in units of counts/(kilorayleigh-pixel).

favors the narrow passband filter by a factor of 1.7. If the filter wheel temperature exceeds the bounds of the usable temperature range, then the moderate passband filters can be employed. For purposes of providing absolute photometry for the auroral emissions at λ391.4 and λ630.0, filters 6 and 7 at λ395.0 and λ626.6, respectively, are included in the filter wheel for imaging photometer A in order to determine background responses from reflected moonlight, etc. The corresponding filter for measuring background emissions for the $[OI]_{32}$ line at λ557.7 is mounted on the filter wheel for imaging photometer B (filter 8, Table II). Imaging photometer A is also capable of providing images of the dayside global ozone distribution with filter 2 which has a passband centered at λ317.5 and passband width of 3.0 nm. Surface albedo for these ozone measurements is determined with a filter at λ360.0. A third filter for ozone measurements at λ317.5 is included in imaging photometer B. Also shown in Table I are the transmissions T_p of each of the twelve filters at their respective wavelengths λ_p of peak transmission and the corresponding absolute sensitivity S_p of imaging photometer A at each of these wavelengths. The photometric sensitivities and filter properties for imaging photometer B are summarized in Table II. Filters for the three auroral emissions λ391.4, λ557.7 and λ630.0 are similar to those for imaging photometer A. In addition imaging photometer B is equipped with a daylight cloud filter at λ629.8 and a filter at λ482.5 that is to be used for surveys of large-scale marine bioluminescence.

The vacuum-ultraviolet imaging photometer C is also provisioned with twelve filters on a filter wheel. Four of these filters are used to image the Lyman-Birge-Hopfield band of molecular nitrogen which is excited by charged particle precipitation and occurs in

the vacuum-ultraviolet window that allows global imaging of the auroral oval in both the dark and sunlit ionospheres. Peak sensitivities S_p are good at these wavelengths and range as high as 2.05 counts/kilorayleigh-pixel for filter 5. Another four filters are included in order to obtain global surveys of the atomic oxygen emissions at λ130.4 and λ135.6 which are also useful for photometric corrections for the auroral N_2(LBH) images. The final four filters with $\lambda_p \approx$ λ125, and $\Delta\lambda \approx$ 10 nm or 30 nm, are dedicated to observations of exospheric hydrogen. The absolute sensitivities of imaging photometer C to hydrogen Lyα emissions at λ121.6 are given as S(Lyα) in Table III.

Thus it is noted above that the three imaging photometers are endowed with considerable operating flexibility to design imaging missions tailored to gain a specific observational objective. For example, during an orbit for which the apogee is at high latitudes and for which the orbital plane lies near the noon-midnight meridional plane, imaging photometer B can be employed to search for marine bioluminescence via filter 7 and photometer A for surveys of mid-latitude red arcs with its filter 11 during the dark, low-altitude portion of the orbit. As sunrise appears at the spacecraft with increasing orbital altitude, the auroral oval will come into view and imaging photometers A and B can be used to gain several continuous hours of monitoring of the morphology of the auroral oval at λ391.4 and λ557.7, respectively. This monitoring of the auroral oval can include occasional image frames with the background filters for absolute photometry. If the low-altitude spacecraft DE-B intercepts a magnetic field line that traverses near the DE-A spacecraft an increase in the temporal resolution for imaging the auroral emissions is gained by commanding both photometers A and B to view λ557.7, for example, with half-width frames. The corresponding frame repetition rate is one frame each 180 s. During this sequence of observations at visible wavelengths the vacuum-ultraviolet imaging photometer C is yielding global images of the auroral emissions of the N_2 (LBH) band which allows viewing of the auroral morphology and dynamics in both the dark and sunlit ionospheres. As the spacecraft descends from apogee to perigee and the sunlit ionosphere is primarily in view, photometer A can be used to assess the global distribution of O_3 while imaging photometer B views the albedo from sunlit cloud cover for a calibration of photometer sensitivity. During this latter period, imaging photometer C can be used to determine asymmetries in the global distribution of exospheric hydrogen. The above imaging sequence is given in order to demonstrate a combination of operating modes for an imaging mission which spans a single orbit. Using the information given here and a readily available ephemeris an investigator should be able to design an imaging mission tailored to particular observational objectives from the large number of combinations of basic instrument operating modes as noted above.

5. Image Processing

Two computer hardware systems are to be utilized in the processing of images obtained from the three imaging photometers for the Dynamics Explorer Mission. These two computers are the Sigma 9 which is located at the Goddard Space Flight Center and

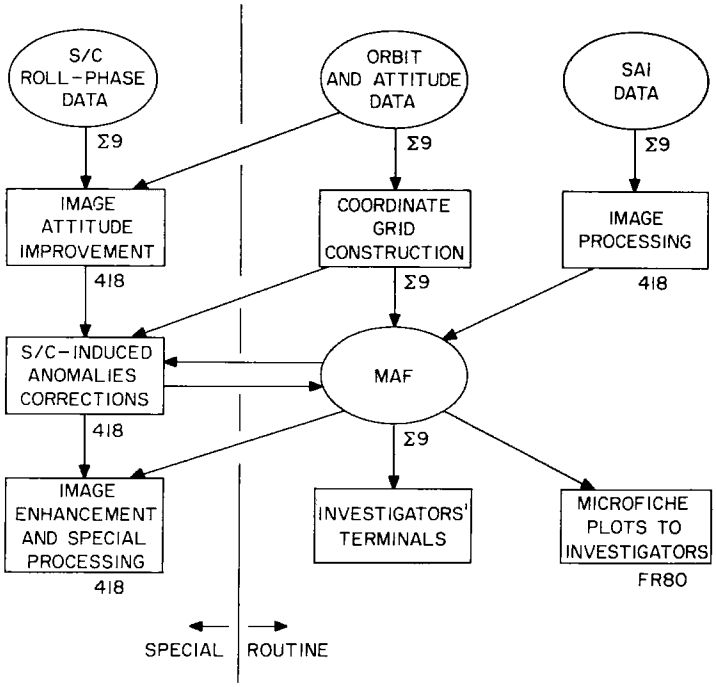

Fig. 9. Summary of the interrelationship of major image processing tasks. The two major computer hardware systems that are employed in the image processing are the Univac 418 at the University of Iowa and the Sigma 9 at the Goddard Space Flight Center.

the Univac 418 facilities at the University of Iowa. Flight operations are expected to create approximately 90 000 images per year. The major elements of the data processing plan for the global auroral imaging investigation are summarized in Figure 9. All images are processed via routine software systems and transferred into the Mission Analysis Files (MAF) [6] for access by the various Dynamics Explorer investigators. This routine processing is depicted on the right-hand side of Figure 9. A typical processed image frame corresponding to a field-of-view of 30 × 30° comprises 1.44 × 10^4 pixels. The photometer responses (SAI data) and spacecraft attitude information which are necessary to reconstruct an image frame are decommutated from the spacecraft telemetry stream by the Sigma 9 and sent via a 9600-baud telecommunications link to the Univac 418. The Univac-418 software allows the pixel arrays which are gained by the combination of mirror scanning and spacecraft rotation to be reconstructed into an image frame. These images are subsequently transferred to the MAF. Algorithms which are resident in the Sigma 9 allow an investigator to display the array of pixels in units of sensor responses, i.e., counts/sec, or absolute photometric units (see Tables I, II, and III). The Sigma 9 is also capable of providing a coordinate grid overlay for each of the images. This latitude-longitude grid is available in geographic and tilted-dipole geomagnetic coordinates. The ground track of the low-altitude Dynamics Explorer B and a map of continental coastlines can be overlayed upon the pixel arrays also. All of these overlays are

available to the investigators' terminals via the MAF and associated software. Since several of the investigators' terminals are insufficiently equipped to display and/or copy the images available from the MAF, all images are sent to investigators as microfiche plots generated by a FR-80 which is interfaced to the Sigma 9 [6]. It is pointed out here that these images at this level of processing are direct reconstructions of the photometer responses and that this reconstruction relies upon nominal performance of the spacecraft attitude-determination electronic systems. These images are extremely useful for correlations with and initial analyses of measurements with companion instruments; however images intended for publication and absolute photometry require special processing.

The relationship of the special imaging processing to be carried out at the University of Iowa with the routine processing as summarized above is shown in Figure 9. Software for the Univac 418 is employed to achieve a pointing accuracy $\leqslant 0.12°$ relative to an earth-referenced coordinate system for each pixel. Knowledge of the spacecraft orbital position and spin axis attitude, and telemetry from the spacecraft roll-phase instruments which are body-mounted infrared horizon sensors and solar aspects sensors, is necessary to determine accurately the viewing directions of the imaging photometers. If there is a malfunction, sporadic or persistent, of the spacecraft attitude-determination systems such that the nominal accuracy for the direction corresponding to a given pixel is not achieved, then further software is required to correct the positioning of a given pixel in an image frame. This further processing is noted as spacecraft-induced anomalies corrections in Figure 9. These image frames with improved determinations of the directions for the photometer fields-of-view are subsequently used to update the MAF, if the quality of the attitude determination is significantly better than that achieved by routine processing. Visual monitoring of the quality of reconstructed images which are produced by routine or special processing is accomplished with an Advent Model 1100 large-screen projection system driven with an 8-bit color-coded Ramtek memory array with dimensions 512×512 pixels. It should be noted that major failures of spacecraft attitude systems can render image reconstruction extremely difficult, if not impossible. Examples of such failures are electronic inoperability of the body-mounted horizon sensors and large-angle, $>0.5°$, motions of the spacecraft spin axis within a frame repetition period.

Image enhancement and special processing are to be employed for images of interest to the detailed analyses by the Dynamics Explorer investigators. These capabilities include improvement of image contrast and visual resolution with (1) fast-Fourier transform, (2) increased dimensions of the displayed pixel array by two-dimensional nonlinear interpolation and (3) tailored color- or gray-coding of response ranges to achieve the optimum performance of the film or screen medium. Additional computer software can provide corrections for stray and background light levels when measurements from the background light filters are available. Hence absolute photometric images of various emissions on a global scale can be achieved. On numerous occasions the imaging photometers are to be operated in modes such that near-simultaneous images of the earth at several wavelengths are acquired. These images are superposed to yield a true-color image of the earth. The images obtained from these image enhancement and

special processing software routines are expected not only to greatly enhance our knowledge of the earth's ionosphere and near-earth magnetosphere when used in correlation with measurements from the companion instrumentation on the two spacecraft, but to yield striking and exciting global views of the dim-light emissions of earth.

Acknowledgements

The design and fabrication of new scientific instrumentation such as these specially designed auroral imaging photometers require a highly motivated, multitalented research staff. We are fortunate to possess such a staff, all of whom deserve recognition. A sincere and grateful thank you to Messrs K. D. Barkalow, M. L. Cannon, R. E. Creque, R. L. Holmes, E. T. Howard, J. A. Lee, H. D. Owens, G. L. Pickett, D. B. Smith, Ms S. K. Miller, and Drs R. J. DeCoster and T. E. Eastman. The assistance of our programming staff, Mr P. E. Moore, and Mss M. R. Dvorsky and N. A. Passo, is gratefully acknowledged. Within the department we received invaluable support in electronics design efforts from Mr J. R. Phillips and Dr D. C. Enemark, in electronics assembly from Ms R. M. Wenman and her staff, in hardware fabrication from Messrs. E. A. Freund, R. M. Markee and the machine-stop staff, and in computer-interface software from Mr R. L. Brechwald.

We wish to thank all members of the Dynamics Explorer project office at the Goddard Space Flight Center for their efforts throughout the program, and to recognize contributions by the project scientist, Dr R. A. Hoffman, the instrument manager, Mr K. D. Fellerman, and the instrument engineer, Mr J. M. Lidston. We acknowledge the substantial support provided by Messrs. J. F. Osantowski (optical designs), J. P. Marshburn and D. Butler (thermal designs), R. G. Martin (electronic systems), J. J. Hirschfield (radiation tests) and Dr B. Seidenberg (materials). To Ms G. M. Miller (thermal-control paints) and Mr N. R. Beard (EPET software) we owe a special thank you for their generous contributions.

In the course of the project we have worked with numerous excellent subcontractors and distributors who provided us subsystems, parts and services. We wish to thank specifically Mr E. Barr (Barr Associates, Inc.), Mr C. V. Muffoletto (Muffoletto Optical Co.), Mr B. K. Flint (Acton Research Corp.), Mr J. H. Vowells (Martin-Marietta Aerospace) and Mr J. Eisenberg (Almag Plating Corp.). Special acknowledgements are due Mr E. Schaeffer (Schaeffer Magnetics, Inc.) and Mr M. T. Spencer (Speedring Systems) for the quality of their work and their keen personal interest throughout the project.

Mr C. K. Garrod of the Scripps Institution of Oceanography is responsible for bringing to our attention the possibility of making a contribution to the study of marine bioluminescence in the open oceans. He will pursue this topic as part of his graduate work. Mr G. M. Keating of NASA/Langley has assisted us in defining appropriate filter characteristics for the total ozone survey.

This effort would have not been possible without the continued support and encouragement from the staff of NASA Headquarters, in particular that of Dr F. D. Martin,

Director, Solar Terrestrial and Astrophysics Division, Dr H. Glaser, former Director, Solar Terrestrial Division, Dr D. P. Cauffman, initial Program Scientist and Dr E. R. Schmerling, current Program Scientist.

This research was supported in part by the National Aeronautics and Space Administration under contract NAS5-24293 and grant NGL 16-001-002 and by the Office of Naval Research under grant N00014-76-C-0016.

References

1. Anger, C. D., Fancott, T., McNally, J., and Kerr, H. S.: *Appl. Opt.* **12**, 1753 (1973).
2. Shepherd, G. G., Fancott, T., McNally, J., and Kerr, H. S.: *Appl. Opt.* **12**, 1767 (1973).
3. Rogers, E. H., Nelson, D. F., and Savage, R. C.: *Science* **183**, 951 (1974).
4. Berkey, F. T. and Kamide, Y.: *J. Geophys. Res.* **81**, 4701 (1976).
5. Kaneda, E.: *Proceedings of the International Workshop on Selected Topics of Magnetospheric Physics*, Japanese IMS Committee, Tokyo, p. 15. (1979).
6. Smith, Paul H., Freeman, Clyde H., and Hoffman, R. A.: *Space Sci. Instr.* **5**, 561 (1981) (this issue).